IV International Conference on Computational Methods for Coupled Problems in Science and Engineering
COUPLED PROBLEMS 2011
M. Papadrakakis, E. Oñate and B. Schrefler (Eds)

PARTITIONED TIME INTEGRATION METHODS FOR HARDWARE IN THE LOOP BASED ON LINEARLY IMPLICIT L-STABLE ROSENBROCK METHODS

ORESTE S. BURSI[*], CHUANGUO JIA[†], ZHEN WANG[*]

[*] Department of Mechanical and Structural Engineering
University of Trento
Via Mesiano 77, 38123 Trento, Italy
e-mail: oreste.bursi@ing.unitn.it, www.ing.unitn.it/~bursi/

[†]School of Civil Engineering, Chongqing University, Chongqing, China

Key words: Real-time, Rosenbrock integration methods, Interfield partitioned methods, Hardware-in-the-loop test.

Abstract. Hardware in the loop based on dynamic substructuring was conceived to be a hybrid numerical-experimental technique to simulate the non-linear behaviour of an emulated structure. Its challenge is to ensure that both numerical and physical substructures interact in real time by means of actuators –transfer systems-. With this objective in mind, the development and implementation of partitioned real-time compatible Rosenbrock algorithms are presented in this paper. In detail, we shortly introduce monolithic linearly implicit L-stable algorithms with two stages; and in view of the analysis of complex emulated structures, we present a novel interfield partitioned algorithm. Both the stability and accuracy properties of the proposed algorithm are examined through analytical and numerical studies carried out on Single-DoF model problems. Moreover, a novel test rig conceived to perform both linear and nonlinear substructure tests is introduced, and tests on a two-DoF split-mass system are illustrated. The drawbacks of this algorithm are underlined and improvements are introduced on a companion solution procedure.

1 INTRODUCTION

In recent years real-time hybrid testing techniques, as depicted in Figure 1, like the Hardware-in-the-Loop (HiL) technique with Dynamic Substructuring (DS), became more and more popular in order to study the performance of components and structures subject to dynamic loads [1,2]. With regard to relevant time-stepping methods, they can be broadly classified in monolithic and partitioned. In a monolithic approach, the method integrates: i) the Numerical Substructure (NS) only, whilst the Physical Substructure (PS) is considered a black box [2]; ii) both the NS and the PS by means of stiffness estimates [3], like in a typical pseudo-dynamic (PsD) test [2]. Conversely, a partitioned approach solves both NS and PS through different integrators and takes into account the interface problem, for instance by prediction, substitution and synchronization of Lagrange multipliers. In detail, partitioned

algorithms can be applied to the Euler-Lagrange form of the equations of motion -second-order in time- [4-6] or to the Hamilton form of the equations of motion -first-order in time- [7,8]. In this paper, we consider partitioned approaches based on L-stable two-stages real-time compatible Rosenbrock (LSRT) algorithms applied to equations of motion first-order in time.

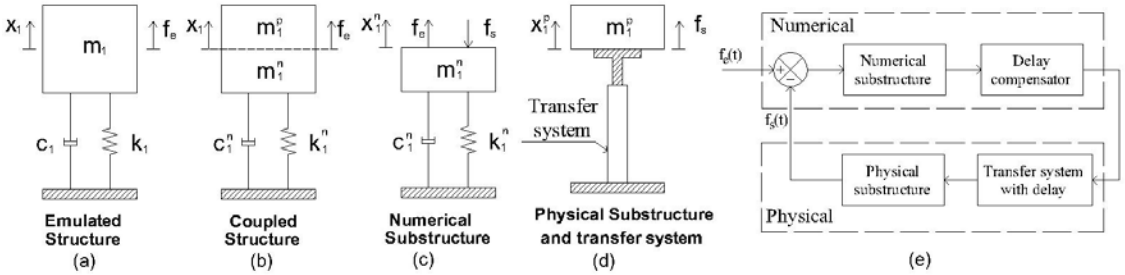

Figure 1: (a)-(d) Schematic representation of a SDoF split-mass system; (e) block diagram representation including delay.

Most of the research works carried out on substructure tests considered structural integrators applied to the equations of motion second-order in time. Nonetheless, it is well known that the motion of a PS in a substructure test, see Fig.1d, is driven by a transfer system –actuator- and sensors, governed by a control unit. Since the control system is typically described by first-order Differential Equations, the utilized integrators have to deal with mixed first- and second-order ODEs. In order to solve this problem, we suggest to employ first-order integrators like the LSRT Rosenbrock algorithms, both for structural and control systems, owing to the favourable properties of LSRT algorithms employed in control [9].

With regard to complex emulated structures, numerical and control requirements impose different time steps for a NS and a PS, respectively. As a result, two main techniques can be identified to tackle this problem: i) model reduction, that represents an effective way to lower computation burdens related to the integration of a complex NS, but becomes very inaccurate especially for non-linear systems; ii) multi-time methods that allow to employ different time integrators in distinct subdomains. Furthermore, subcycling permits to use different time steps in different subdomains. The last strategy is relatively simple to implement, but it can hinder stability and accuracy properties of the original schemes. Therefore, the paper proposes some novel multi-time method with subcycling strategies, investigates relevant stability and accuracy issues and presents hardware-in-the-loop tests. Also, limits and remedies of the treated multi-time method are suggested.

The remaining part of the paper is organized as follows. Firstly, LSRT algorithms with two stages (LSRT2) are introduced, which are nowadays used in real-time substructured tests [10], as an alternative to structural integrators applied to the equations of motion second-order in time [11,12]. Then, interfield parallel algorithms with subcycling strategies based on the progenitor LSRT algorithm that represent the main focus of the paper are considered. These linearly implicit algorithms first solve the interface problem by means of Lagrange multipliers and subsequently advance the solution in all subdomains. Thus, stability and accuracy properties of these algorithms are analysed through numerical experiments on a Single-DoF split-mass system, including subcycling too. Successively, real-time tests conducted by means of a novel test rig on a two-DoF systems are presented and commented. The limits of this algorithm are underlined and improvements are introduced on a companion interfield parallel

solution procedure. Lastly, main conclusions are drawn.

2 LINEARLY IMPLICIT ROSENBROCK-BASED ALGORITHMS

In this section, we introduce the LSRT compatible algorithms developed and suggested by Bursi et al. [10]. They are linearly implicit because eliminate the need to solve non-linear systems for nonlinear problems. To employ LSRT algorithms, the equations of motion

$$\mathbf{M}\ddot{\mathbf{u}} = \mathbf{r}\left(\mathbf{u},\dot{\mathbf{u}},t\right) \tag{1}$$

can be rewritten into a state-space form

$$\dot{\mathbf{y}} = \mathbf{f}\left(\mathbf{y},t\right),\ \text{with}\ \mathbf{y} = \begin{Bmatrix}\mathbf{u}\\ \dot{\mathbf{u}}\end{Bmatrix},\ \mathbf{f}\left(\mathbf{y},t\right) = \begin{Bmatrix}\dot{\mathbf{u}}\\ \mathbf{r}\left(\mathbf{u},\dot{\mathbf{u}},t\right)\end{Bmatrix}, \tag{2}$$

where **M** stands for the mass matrix which is assumed to be symmetric positive definite for simplicity $\mathbf{f}\left(\mathbf{y},t\right)$ and $\mathbf{r}\left(\mathbf{u},\dot{\mathbf{u}},t\right)$ for the vectors of applied and internal forces, respectively. In a FE context, the force vector can be split as $\mathbf{r}\left(\mathbf{u},\dot{\mathbf{u}},t\right) = -\mathbf{K}\mathbf{u} - \mathbf{C}\dot{\mathbf{u}} + \mathbf{F}_e$ with a stiffness matrix **K**, a damping matrix **C** and a displacement vector **u**. Differentiation with respect to time is expressed by a dot, and thus we set $\dot{\mathbf{u}}$ and $\ddot{\mathbf{u}}$ to define the corresponding velocity and acceleration vectors.

The two-stage L-stable real-time two-stage (LSRT2) method applied to $\dot{\mathbf{y}} = \mathbf{f}\left(\mathbf{y},t\right)$ reads:

$$\mathbf{k}_1 = \left[\mathbf{I} - \gamma\Delta t\mathbf{J}\right]^{-1}\mathbf{f}\left(\mathbf{y}_k,t_k\right)\Delta t,\ \ \mathbf{y}_{k+\alpha_{21}} = \mathbf{y}_k + \alpha_{21}\mathbf{k}_1, \tag{3}$$

$$\mathbf{k}_2 = \left[\mathbf{I} - \gamma\Delta t\mathbf{J}\right]^{-1}\left(\mathbf{f}\left(\mathbf{y}_{k+\alpha_{21}},t_{k+\alpha_2}\right) + \mathbf{J}\gamma_{21}\mathbf{k}_1\right)\Delta t,\ \ \mathbf{y}_{k+1} = \mathbf{y}_k + b_1\mathbf{k}_1 + b_2\mathbf{k}_2, \tag{4}$$

where Δt is the step interval and $\mathbf{J} = \left(\partial\mathbf{f}/\partial\mathbf{y}\right)$ is the Jacobian matrix evaluated at the first stage. Two sets of parameters that satisfy second-order accuracy, L-stability and real-time compatibility are introduced, namely $\gamma = 1 - \sqrt{2}/2$ and $\gamma = 1 + \sqrt{2}/2$, respectively, together with $\alpha_2 = \alpha_{21} = 1/2$, $\gamma_{21} = -\gamma$, $b_1 = 0$ and $b_2 = 1$. The favourable performance of the LSRT2 method with respect to low and high-frequency components of the response can be observed from Figure 2, where a comparison with the Generalized-α [13] method is illustrated.

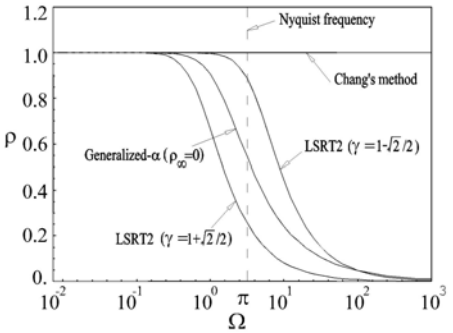

Figure 2: Spectral radii ρ of linearly implicit algorithms with respect to the Generalized-α method vs. the non-dimensional frequency Ω.

3 A PARTITIONED TIME INTEGRATION METHOD BASED ON ACCELERATION CONSTRAINT

In this section, we present a partitioned time integration method that adopts both element-based partitioning and the LSRT2 method presented in Section 2. Due to real-time compatibility, we consider the acceleration continuity at the interface of subdomains, and therefore, an explicit Lagrange multiplier formulation is obtained. Moreover, the novel partitioned method preserves favourable second-order accuracy, and very often, both unconditionally stability and high-frequency dissipation capabilities.

3.1 Derivation of an explicit Lagrange multiplier vector

In order to implement the LSRT2 method, we begin with a system of index one

$$\begin{cases} \begin{bmatrix} \mathbf{I} & \mathbf{0} \\ \mathbf{0} & \mathbf{M}^i \end{bmatrix} \begin{Bmatrix} \dot{\mathbf{u}}^i \\ \ddot{\mathbf{u}}^i \end{Bmatrix} = \begin{Bmatrix} \dot{\mathbf{u}}^i \\ \mathbf{f}\left(\mathbf{u}^i, \dot{\mathbf{u}}^i, t\right) \end{Bmatrix} + \begin{bmatrix} \mathbf{0} \\ (\mathbf{G}^i)^T \end{bmatrix} \mathbf{\Lambda} \qquad i = 1, ..., S \\ \sum_{i=1}^{S} \begin{bmatrix} \mathbf{0}, \mathbf{G}^i \end{bmatrix} \begin{Bmatrix} \dot{\mathbf{u}}^i \\ \ddot{\mathbf{u}}^i \end{Bmatrix} = \mathbf{0} \end{cases}, \tag{5}$$

which is modelled as a set of S non-overlapping subdomains constrained by acceleration continuity at the interface. For simplicity, we only consider the case with linear constraint equations [14]. With the assumption $\mathbf{y} = \left\{ \mathbf{u}^T \quad \dot{\mathbf{u}}^T \right\}^T$, one obtains

$$\begin{cases} \mathbf{A}^i \dot{\mathbf{y}}^i = \mathbf{F}^i \left(\mathbf{y}^i, t \right) + (\mathbf{C}^i)^T \mathbf{\Lambda} \\ \sum_{i=1}^{S} \mathbf{C}^i \dot{\mathbf{y}}^i = \mathbf{0} \end{cases}, \tag{6}$$

For easiness of notation, both the matrices $\mathbf{A}^i$ and $\mathbf{C}^i$ refer to the i-th subdomain. Both the vector $\dot{\mathbf{y}}^i$ and the Lagrange multiplier vector $\mathbf{\Lambda}$ can be explicitly solved by means of (6), i.e.

$$\dot{\mathbf{y}}^i = (\mathbf{A}^i)^{-1} \mathbf{F}^i \left(\mathbf{y}^i, t \right) + (\mathbf{A}^i)^{-1} (\mathbf{C}^i)^T \mathbf{\Lambda} \tag{7}$$

with

$$\mathbf{\Lambda} = -\mathbf{H}^{-1} \sum_{i=1}^{S} \mathbf{C}^i (\mathbf{A}^i)^{-1} \mathbf{F}^i \left(\mathbf{y}^i, t \right) \tag{8}$$

and

$$\mathbf{H} = \sum_{i=1}^{S} \mathbf{C}^i (\mathbf{A}^i)^{-1} (\mathbf{C}^i)^T . \tag{9}$$

Equations (7) and (8) can be expressed in compact forms as

$$\dot{\mathbf{y}} = \mathbf{A}^{-1} \mathbf{F} \left(\mathbf{y}, t \right) + \mathbf{A}^{-1} \mathbf{C}^T \mathbf{\Lambda} \tag{10}$$

with

$$\mathbf{\Lambda} = -\left[\mathbf{C}\mathbf{A}^{-1}\mathbf{C}^{T}\right]^{-1}\mathbf{C}\mathbf{A}^{-1}\mathbf{F}\left(\mathbf{y},t\right), \tag{11}$$

where

$$\begin{aligned}&\mathbf{y} = \left\{(\mathbf{y}^1)^T \quad ... \quad (\mathbf{y}^S)^T\right\}^T, \qquad \mathbf{A} = \text{Blockdiagonal}[\mathbf{A}^1 \quad ... \quad \mathbf{A}^S]\\ &\mathbf{F}\left(\mathbf{y},t\right) = \left\{\left[\mathbf{F}^1\left(\mathbf{y}^1,t\right)\right]^T \quad ... \quad \left[\mathbf{F}^S\left(\mathbf{y}^S,t\right)\right]^T\right\}^T, \quad \mathbf{C} = [\mathbf{C}^1 \quad ... \quad \mathbf{C}^S]\end{aligned}. \tag{12}$$

Hence, the proposed partitioned method is based on the explicit evaluation of $\mathbf{\Lambda}$ at the beginning of each time step/stage, and thus, the integration of each subdomain can independently advance.

3.2 Solution procedure of partitioned time integration methods

For simplicity, let us consider a system divided into two subdomains A and B. In the case that both subdomains be integrated by the LSRT2 algorithm with the same time step Δt, i.e. ss=1, the solution procedure of the partitioned method can be represented as in Figure 3, endowed with the task numbering. In detail, it can be characterized as follows:

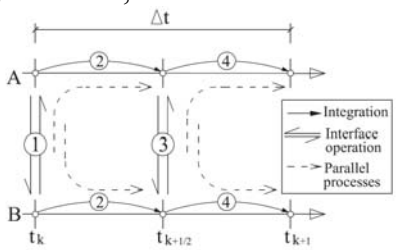

Figure 3 : The procedure of the LSRT2-based partitioned parallel method with ss=1

(1) Evaluate $\mathbf{F}_k^A$ and $\mathbf{F}_k^B$ and calculate the Lagrange multiplier $\mathbf{\Lambda}_k$ at time t_k,

$$\mathbf{\Lambda}_k = -\mathbf{H}^{-1}\left[\mathbf{C}^A(\mathbf{A}^A)^{-1}\mathbf{F}_k^A + \mathbf{C}^B(\mathbf{A}^B)^{-1}\mathbf{F}_k^B\right]. \tag{13}$$

(2) Compute $\mathbf{k}_1^i$ where $i = A, B$ and evaluate the solutions $\mathbf{y}_{k+1/2}^i$ ($i = A, B$) -First stage-

$$\mathbf{k}_1^i = \left[\mathbf{I} - \gamma\Delta t\mathbf{J}^i\right]^{-1}(\mathbf{A}^i)^{-1}\left[\mathbf{F}_k^i + (C^i)^{-1}\mathbf{\Lambda}_k\right]\Delta t, \tag{14}$$

$$\mathbf{y}_{k+1/2}^i = \mathbf{y}_k^i + \frac{1}{2}\mathbf{k}_1^i. \tag{15}$$

(3) Evaluate $\mathbf{F}_{k+1/2}^A$ and $\mathbf{F}_{k+1/2}^B$ and calculate $\mathbf{\Lambda}_{k+1/2}$ at time $t_{k+1/2}$,

$$\mathbf{\Lambda}_{k+1/2} = -\mathbf{H}^{-1}\left[\mathbf{C}^A(\mathbf{A}^A)^{-1}\mathbf{F}_{k+1/2}^A + \mathbf{C}^B(\mathbf{A}^B)^{-1}\mathbf{F}_{k+1/2}^B\right]. \tag{16}$$

(4) Compute $\mathbf{k}_2^i$ and advance the solution to $\mathbf{y}_{k+1}^i$ in both subdomains, respectively, -Second

stage-

$$\mathbf{k}_2^i = \left[\mathbf{I} - \gamma \Delta t \mathbf{J}^i\right]^{-1} (\mathbf{A}^i)^{-1} \left[\mathbf{F}_{k+1/2}^i + (C^i)^{-1} \mathbf{\Lambda}_{k+1/2} - \gamma \mathbf{J}^i \mathbf{k}_1^i\right] \Delta t \,, \tag{17}$$

$$\mathbf{y}_{k+1}^i = \mathbf{y}_k^i + \mathbf{k}_2^i \,. \tag{18}$$

Since the LSRT2 method contains two stages, inter-domain exchange of information is not only required at the beginning of each time step, but also at the beginning of the second stage. This algorithm can be defined as parallel, because the interconnection is only done at the beginning of each stage to compute the Lagrange multiplier; then each subdomain can independently advance in each stage.

4 AN INTERFIELD PARALLEL SOLUTION PROCEDURE

Along the line of [6], the Rosenbrock-based method developed above can be exploited to develop an interfield parallel procedure. To illustrate that, let us consider again two subdomains A and B. The solution procedure is highlighted in Figure 4 with the numbering of the two processes and the subscript i referred to the time step Δt. In detail, Subdomain A is integrated with the coarse time step $\Delta t_A = 4 \cdot \Delta t$, while Subdomain B with the fine time step $\Delta t_B = \Delta t / ss$, where $ss = 2$. The solution procedure for Subdomain A is as follows:

(1) Evaluate $\mathbf{F}_{i-2}^A$ and $\mathbf{F}_{i-2}^B$ with the solutions $\mathbf{y}_{i-2}^A$ and $\mathbf{y}_{i-2}^B$ and then calculate the Lagrange multiplier $\mathbf{\Lambda}_{i-2}$,

$$\mathbf{\Lambda}_{i-2} = -\mathbf{H}^{-1} \left[\mathbf{C}^A \left(\mathbf{A}^A \right)^{-1} \mathbf{F}_{i-2}^A + \mathbf{C}^B \left(\mathbf{A}^B \right)^{-1} \mathbf{F}_{i-2}^B \right]. \tag{19}$$

(2) Compute $\mathbf{k}_1^A$ and advance the solution to $\mathbf{y}_i^A$,

$$\mathbf{k}_1^A = \left[\mathbf{I} - 4\Delta t \gamma \mathbf{J}^A\right]^{-1} \left(\mathbf{A}^A\right)^{-1} \left[\mathbf{F}_{i-2}^A + \left(\mathbf{C}^A\right)^T \mathbf{\Lambda}_{i-2}\right] 4\Delta t \,, \tag{20}$$

$$\mathbf{y}_i^A = \mathbf{y}_{i-2}^A + \frac{1}{2} \mathbf{k}_1^A \,. \tag{21}$$

(3) Evaluate $\mathbf{F}_i^A$ and $\mathbf{F}_i^B$ and then calculate $\mathbf{\Lambda}_i$,

$$\mathbf{\Lambda}_i = -\mathbf{H}^{-1} \left[\mathbf{C}^A \left(\mathbf{A}^A \right)^{-1} \mathbf{F}_i^A + \mathbf{C}^B \left(\mathbf{A}^B \right)^{-1} \mathbf{F}_i^B \right]. \tag{22}$$

(4) Evaluate $\mathbf{k}_2^A$ and advance the solution to $\mathbf{y}_{i+2}^A$,

$$\mathbf{k}_2^A = \left[\mathbf{I} - 4\Delta t \gamma \mathbf{J}^A\right]^{-1} \left\{ \left(\mathbf{A}^A\right)^{-1} \left[\mathbf{F}_i^A + \left(\mathbf{C}^A\right)^T \mathbf{\Lambda}_i\right] - \gamma \mathbf{J}^A \mathbf{k}_1^A \right\} 4\Delta t \,, \tag{23}$$

$$\mathbf{y}_{i+2}^A = \mathbf{y}_i^A + \mathbf{k}_2^A \,. \tag{24}$$

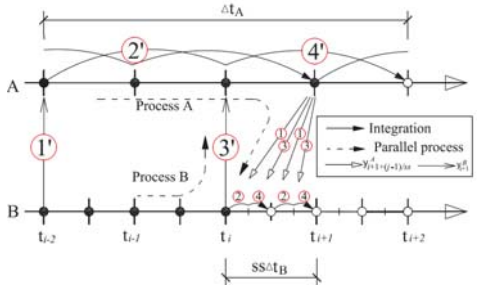

Figure 4 The interfield parallel procedure of the LSRT2-based partitioned method with *ss*=2.

(5) Calculate $\mathbf{y}^A_{i+1+\frac{in}{2ss}}$ by means of linear interpolation:

$$\mathbf{y}^A_{i+1+\frac{in}{2ss}} = \left(1-\frac{in}{2ss}\right)\mathbf{y}^A_{i+1} + \frac{in}{2ss}\mathbf{y}^A_{i+2}, \quad \left(in = 1,2,....,2ss\right). \tag{25}$$

At the same time, the advancement procedure for $\left(j = 1,...,s\right)$ substep in subdomain B, i.e. from $\mathbf{y}^B_i$ to $\mathbf{y}^B_{i+1}$ reads:

(1) Evaluate $\mathbf{F}^A_{i+\frac{j-1}{ss}}$ and $\mathbf{F}^B_{i+\frac{j-1}{ss}}$ and calculate $\mathbf{\Lambda}_{i+\frac{j-1}{ss}}$,

$$\mathbf{\Lambda}_{i+\frac{j-1}{ss}} = -\mathbf{H}^{-1}\left[\mathbf{C}^A\left(\mathbf{A}^A\right)^{-1}\mathbf{F}^A_{i+\frac{j-1}{ss}} + \mathbf{C}^B\left(\mathbf{A}^B\right)^{-1}\mathbf{F}^B_{i+\frac{j-1}{ss}}\right]. \tag{26}$$

(2) Calculate $\mathbf{k}^B_1$ and advance the solution to $\mathbf{y}^B_{i+\frac{2j-1}{2ss}}$,

$$\mathbf{k}^B_1 = \left[\mathbf{I}-\frac{\Delta t}{ss}\gamma\mathbf{J}^B\right]^{-1}\left(\mathbf{A}^B\right)^{-1}\left[\mathbf{F}^B_{i+\frac{j-1}{ss}} + \left(\mathbf{C}^B\right)^T\mathbf{\Lambda}_{i+\frac{j-1}{ss}}\right]\frac{\Delta t}{ss}, \tag{27}$$

$$\mathbf{y}^B_{i+\frac{2j-1}{ss}} = \mathbf{y}^B_{i+\frac{j-1}{ss}} + \frac{1}{2}\mathbf{k}^B_1. \tag{28}$$

(3) Evaluate $\mathbf{F}^A_{i+\frac{2j-1}{2ss}}$ and $\mathbf{F}^B_{i+\frac{2j-1}{2ss}}$ and calculate $\mathbf{\Lambda}_{i+\frac{2j-1}{2ss}}$,

$$\mathbf{\Lambda}_{i+\frac{2j-1}{2ss}} = -\mathbf{H}^{-1}\left[\mathbf{C}^A\left(\mathbf{A}^A\right)^{-1}\mathbf{F}^A_{i+\frac{2j-1}{2ss}} + \mathbf{C}^B\left(\mathbf{A}^B\right)^{-1}\mathbf{F}^B_{i+\frac{2j-1}{2ss}}\right]. \tag{29}$$

(4) Calculate $\mathbf{k}^B_2$ and advance the solution to $\mathbf{y}^B_{i+\frac{j+1}{ss}}$,

$$\mathbf{k}^B_2 = \left[\mathbf{I}-\frac{\Delta t}{ss}\gamma\mathbf{J}^B\right]^{-1}\left\{\left(\mathbf{A}^B\right)^{-1}\left[\mathbf{F}^B_{i+\frac{2j-1}{2ss}} + \left(\mathbf{C}^B\right)^T\mathbf{\Lambda}_{i+\frac{2j-1}{2ss}}\right] - \gamma\mathbf{J}^B\mathbf{k}^B_1\right\}\frac{\Delta t}{ss}, \tag{30}$$

$$\mathbf{y}^B_{i+\frac{j}{ss}} = \mathbf{y}^B_{i+\frac{j-1}{ss}} + \mathbf{k}^B_2. \tag{31}$$

The method is not self-starting and to preserve second-order accuracy and parallel characteristics, we have chosen the LSRT2-based partitioned method with no subcycling to initiate the procedure.

5 NUMERICAL SIMULATIONS AND HARDWARE-IN-THE-LOOP TESTS

In order to examine numerical properties of the newly-developed method, spectral stability and convergence are analysed on a Single-Dof split mass system. Additionally, results provided with Hardware-in-the-loop tests on a two-Dof system are presented as well.

5.1 Stability and convergence analysis on a Single-Dof split mass system

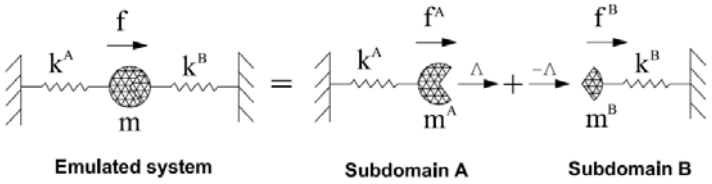

Figure 5: A Single-DoF emulated system with the relevant split-mass system.

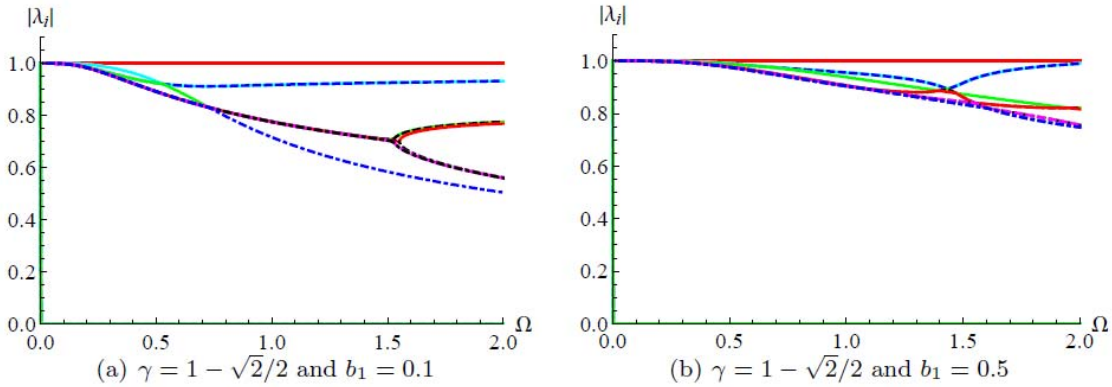

Figure 6: $|\lambda_i|$ of the SDoF problem for the interfield parallel procedure with *ss*=10 and (a) b_1=0.1, $\gamma = 1-\sqrt{2}/2$; (b) b_1=0.5, $\gamma = 1-\sqrt{2}/2$.

We consider the test problem depicted in Figure 5. For simplicity, we choose the following system variables $m = m_A + m_B = 1$ and $k = k_A + k_B = 1$; and b_1 defined as

$$b_1 = \frac{m_A}{m_B} = \frac{k_B}{k_A}. \tag{32}$$

In order to highlight the numerical dissipation properties of the method on the solution, we consider no physical damping. Moreover, no external force is involved as well. The application of the integration methods to this model problem leads to the recursive formula

$$\mathbf{y}_{k+1} = \mathbf{R}\mathbf{y}_k + \mathbf{L}_k, \tag{33}$$

where **R** is the amplification matrix and **L** is the load vector that depends on external forces, respectively. The spectral stability of the method is analysed through the spectral eigenvalues $|\lambda_i|$ of **R.**

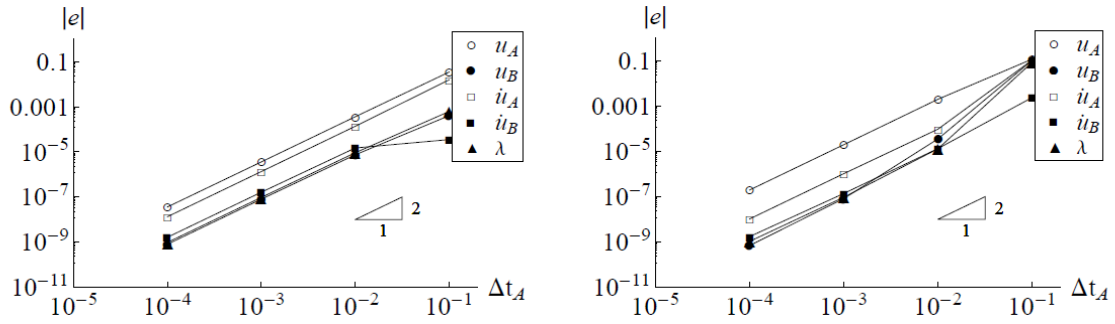

Figure 7: Global errors of the inter-field parallel method with ss=10 and (a) $\gamma = 1-\sqrt{2}/2$; (b) $\gamma = 1+\sqrt{2}/2$

The parallel method is not self-starting and therefore the choice of proper state variables for the stability analysis represents the main difficulty. The initial solutions are composed of $\mathbf{y}_{k-2}^A, \mathbf{y}_{k-2}^B, \mathbf{y}_k^A, \mathbf{y}_k^B$ and $\mathbf{y}_{k+1}^A$,while the output contains only $\mathbf{y}_{k+1}^B$ and $\mathbf{y}_{k+2}^A$. Moreover, another pair of intermediate solutions $\mathbf{y}_{k-1}^A$, $\mathbf{y}_{k-1}^B$ are needed. As a result, the state vector involved in the spectral stability analysis reads

$$\mathbf{X}_k = \left[\left(\mathbf{y}_{k-2}^A\right)^T \quad \left(\mathbf{y}_{k-2}^B\right)^T \quad \left(\mathbf{y}_{k-1}^A\right)^T \quad \left(\mathbf{y}_{k-1}^B\right)^T \quad \left(\mathbf{y}_k^A\right)^T \quad \left(\mathbf{y}_k^B\right)^T \quad \left(\mathbf{y}_{k+1}^A\right)^T \right]^T. \tag{34}$$

Consequently $\mathbf{X}_k$ has a dimension $8n_A + 6n_B$, with n_A and n_B the DoFs of the two subdomains, respectively. For the single-DoF split-mass system, the dimension is 14. $|\lambda_i|$ relevant to the model problem integrated with the algorithm vs. the numerical frequency $\Omega = \sqrt{k/m}\Delta t_A$ are plotted in Figure 5. The number of nonzero eigenvalues is found to be 10: one is unitary, four pairs of them are complex conjugate and the other one is frequently less than 1. Besides, four zero eigenvalues are included. The method with $\gamma = 1+\sqrt{2}/2$ exhibits unconditional stability, while the one characterized by $\gamma = 1-\sqrt{2}/2$ sometimes is only conditionally stable (see Figure 6). Moreover, the stability of the parallel method depends on the parameter b_1 defined in (32). Larger values of b_1 introduce more damping and render the method more stable. For more information, readers are referred to [8].

Successively, the global error is analysed on the SDoF split mass system with the initial conditions $d(t_0) = 1$ and $v(t_0) = 1$. Figure 7 shows that the order of convergence of state variables is in agreement with the theoretical analysis and hence the method exhibits second-order accuracy [8].

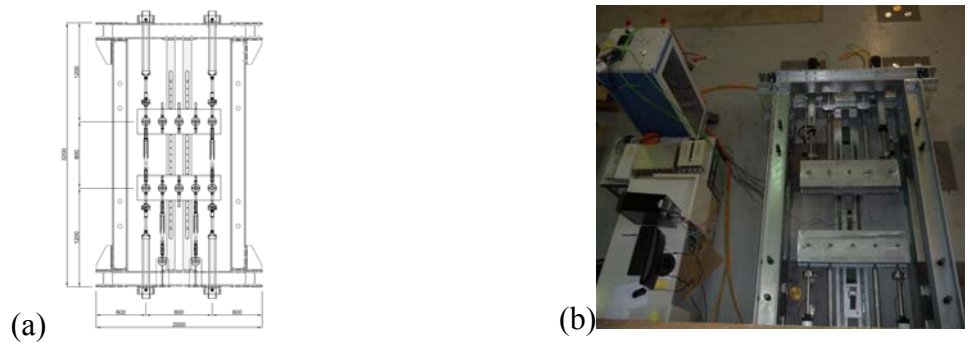

(a) (b)

Figure 8: The test rig : (a) drawing; (b) photo.

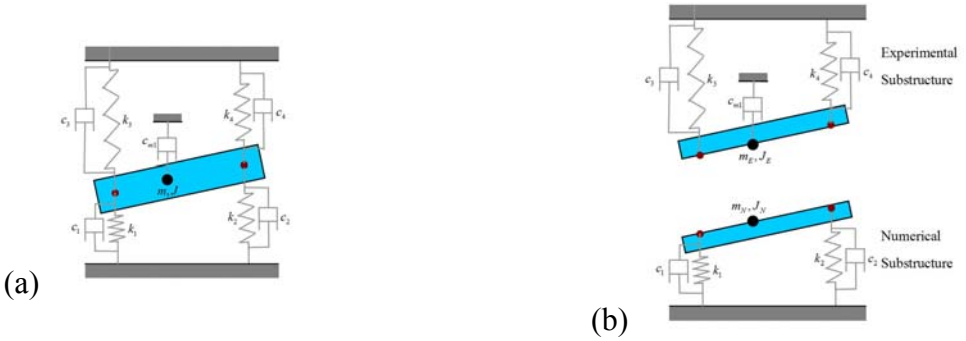

(a) (b)

Figure 9: The simulation model: (a) 2Dof emulated structure; (b) the split system.

5.2 Tests on Two-Dof split-mass system

Table 1: Characteristics of both emulated and split subdomains in Hardware-in-the-loop tests

Struct. types / Properties	Emulated system			Numerical substructure			Physical substructure		
Items	M	K	C	M_N	K_N	C_N	M_P	K_P	C_P
Translational	2210.9	346310	555.66	1658.2	306640	555.66	552.7	39670	0
Rotational	157.2	138524	22.226	117.9	12265	22.226	39.3	1711	0

Note: all valuables are in International Units.

In ordrer to validate the effectiveness of the proposed methods in Hardware-in-the-loop tests, a versatile system was conceived and installed at the University of Trento, Italy. It consists of four actuators, one dSpace DS1103 control board and other high performance devices, shown in Figure 8. This section briefly describes the application of the new parallel method on the 2Dof split mass system, illustrated in Figure 9.

The system characteristics are collected in Table 1. In view of the different sampling times in different subdomains, multitasking techniques are exploited to make most of the advantages of the algorithm, such as multiple rates and parallel implementation. In the test, we selected $\Delta t_A = 4 \cdot \Delta t = 16\text{ms}$ and $\Delta t_B = \Delta t / ss = 2\text{ms}$. Additionally, the system delay of about 20ms was compensated for by means of a polynomial delay compensation scheme [14].

Test results compared with reference numerical simulations are presented in Figure 10. Both displacements fit well to the simulated ones considering the fact that friction forces existing in the system were not modelled. In addition, smaller limited drifts between displacements relevant to both the numerical and the physical substructure were observed.

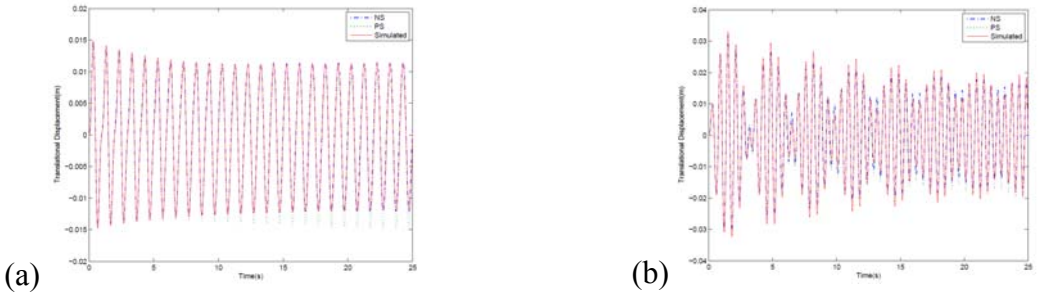

Figure 10: Test results: (a) translational displacement time histories; (b) rotational time histories.

6 AN IMPROVED PARALLEL SOLUTION PROCEDURE

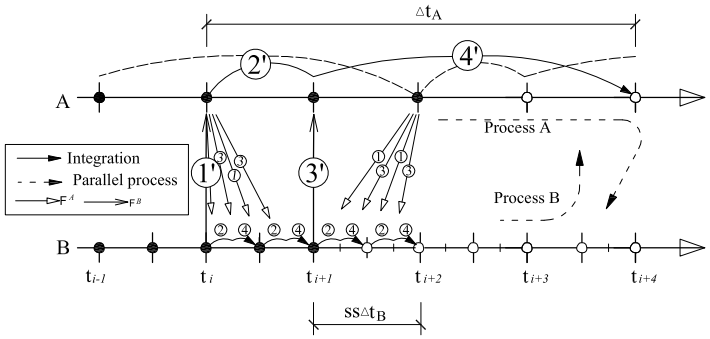

Figure 11: The solution procedure of the improved parallel algorithm

The interfield parallel method presented in Section 4 and tested in Section 5 is appealing, because of its flexibility of dealing with different substructure requirements. Unfortunately, the drift-off effects may limit its applications. Additionally, four parallel integration processes are required for Subdomain A. Based on this insight, the integration method was simplified by conducting the integration in Subdomain A with different stage sizes. Its characteristics can be observed in Figure 11. In addition, displacement drift observed in the progenitor algorithm was reduced via velocity projection at the end of each step [15]. The complete solution procedure of the improved method is also illustrated in Figure 11. Convergence analyses and applications to real-time Hardware-in-the-loop tests will be presented elsewhere.

7 CONCLUSIONS

Initially in this paper, we introduced and applied linearly implicit L-stable Rosenbrock methods with two-stages to real time hardware-in-the-loop substructure tests. The methods are endowed with several favourable characteristics, among which real-time compatibility, explicit evaluation of state variables and user-defined high-frequency dissipation capabilities. In detail and in view of hybrid testing of complex emulated structures, we developed and

illustrated a novel interfield parallel partitioned algorithm based on the progenitor Rosenbrock method, that can incorporate subcycling. Through spectral analysis and numerical simulations on an SDoF split-mass system, both stability and accuracy properties were shown. In a greater detail, the partitioned algorithm preserved second-order accuracy as the progenitor monolithic method and favourable stability properties. Moreover a novel test rig conceived to perform both linear and nonlinear substructure tests was introduced, and tests on a two-DoF split-mass system were illustrated. The drawbacks of this algorithm were commented and improvements were implemented on a companion solution procedure. Finally, these algorithms will allow an in-depth study of errors and control strategies of actuators.

REFERENCES

[1] Saouma V. and Sivaselvan M.V. (Editors) 2008. *Hybrid Simulation - Theory, implementation and applications*, Taylor&Francis, London (2008).

[2] Bursi, O. S. and Wagg, D. J. (Editors). *Modern testing techniques for structural systems –Dynamics and control, Springer*, Wien, New York (2008).

[3] Jung, R. Y., Shing, P. B., Stauffer, E. and Thoen, B. Performance of a real-time pseudodynamic test system considering nonlinear structural response. *Earth. Engng. Struct. Dyn.* (2007), **36**:1785-1809.

[4] Prakash, A. and Hjelmstad, K. D. 2004. A FETI-based multitime-step coupling method for Newmark schemes in structural dynamics. *Int. J. Num. Meth. Engng* (2004) **61**:2183-2204.

[5] Bonelli, A., Bursi, O. S., He, L., Magonette, G. and Pegon, P. Convergence analysis of a parallel interfield method for heterogeneous simulations with substructuring. *Int. J. Num. Meth. Engng* (2008) **75**:800-825.

[6] Bursi O.S., He L., Bonelli, A., Pegon, P., Novel generalized-alpha methods for interfield parallel integration of heterogeneous structural dynamic systems, *J. Comp. Appl. Math*, (2010), **234**:2250-2258.

[7] Nakshatrala, K. B., Hjelmstad, K. D. and Tortorelli, D. A. 2008. A FETI-based domain decomposition technique for time-dependent first-order systems based on a DAE approach. *Int. J. Num. Meth. Engng* (2008) **75**:1385-1415.

[8] Jia C., Bursi, O.S., Bonelli A. and Wang Z., Novel partitioned integration methods for DAE systems based on L-stable linearly implicit algorithms, *Int. J. Num. Meth. Engng* (2011), in print.

[9] Bursi O.S., Stoten D.P., Tondini N., Vulcan L., Stability and accuracy analysis of a discrete model reference adaptive controller without and with time delay, *Int. J. Num. Meth. Engng* (2010) **82**:1158-1179.

[10] Bursi, O.S., Jia C., Vulcan, L., Neild S.A. and Wagg, D. J., Rosenbrock-based algorithms and subcycling strategies for real-time nonlinear substructure testing, *Earth. Engng. Struct. Dyn.* (2011), **40**:1-19.

[11] Chang S. Y. Explicit pseudodynamic algorithm with unconditional stability. *J. Engng. Mech.* (2002), **128**:935-947.

[12] Bursi, O.S. He L., Lamarche C.P. and Bonelli A., Linearly implicit time integration methods for real-time dynamic substructure testing, *J. Engng. Mech.* (2010), **136**:1380-1389.

[13] Chung, J. and Hulbert, G.M. 1993. A time integration algorithm for structural dynamics with improved numerical dissipation: the generalized-alpha method. Journal of Applied Mechanics **60**:371-375.

[14] Lamarche CP. Development of real-time dynamic substructuring procedures for the seismic testing of steel structure. PhD thesis, Universite de Montreal and University of Trento, Italy, 2009.

[15] Bauchau O. A. and Laulusa A. Review of Contemporary Approaches for Constraint Enforcement in Multibody Systems. *J. Comput. Nonlinear Dynam.* **3**: 01-10 (2008).